GEOPHYSICAL RESEARCH LETTERS, VOL. 33, L21501, doi:10.1029/2006GL028342, 2006

Modeling the salinity profile of undeformed Arctic sea ice

Martin Vancoppenolle,[1] Thierry Fichefet,[1] and Cecilia M. Bitz[2]

Received 2 October 2006; accepted 9 October 2006; published 2 November 2006.

[1] The salinity of sea ice affects its physical and ecological properties. Here, a multilayer one-dimensional halo-thermodynamic sea ice model is used to simulate the vertical salinity profile of undeformed Arctic sea ice. The model successfully reproduces the desalination pattern observed in first-year (FY) and multi-year (MY) ice. The model can also be integrated with a prescribed, time-independent salinity profile. Substantial differences in the simulated mass balance and ice-ocean salt flux arise depending on the salinity. After 10 years into the simulation, the annual mean ice thickness is 2.85 m with the interactive halodynamic component, compared to 2.53 m (2.29 m) with a prescribed, time-independent, vertically varying (constant) salinity profile. Modelling sea ice salinity is especially important when sea ice is transitioning from a MY to FY ice regime. Thus including a halodynamic component in sea ice models would significantly improve simulations of future climate. **Citation:** Vancoppenolle, M., T. Fichefet, and C. M. Bitz (2006), Modeling the salinity profile of undeformed Arctic sea ice, *Geophys. Res. Lett.*, *33*, L21501, doi:10.1029/2006GL028342.

1. Introduction

[2] Sea ice is a major component of the climate system and a preferential site for the development of microorganisms and algae [*Ackley and Sullivan*, 1994]. Consequently, the changes in the physical state of the sea ice cover projected for the next century [e.g., *Arzel et al.*, 2006] are likely to have serious repercussions on polar environments and ecosystems.

[3] Sea ice traps some salt as it forms. This salt is contained in brine pockets, while the ice itself is nearly salt-free. The salinity of sea ice S for the combined ice and brine pockets is usually much less than seawater, although the brine pocket salinity alone can be much higher.

[4] The salinity of sea ice plays a significant role in its mass balance and the salt/freshwater exchange between ice and ocean [*Vancoppenolle et al.*, 2005]. The relative volume of salty liquid (brine) inclusions (e) in sea ice strongly depends on ice salinity and temperature. In turn, the sea ice thermal properties depend on e. Above an e = 5% threshold, the brine network becomes interconnected, rendering the sea ice permeable to fluid transport [*Golden et al.*, 1998]. This structural change directly influences the nutrient supply for microorganisms and algae living in sea ice [*Ackley and Sullivan*, 1994] and the atmosphere-ocean exchange of dissolved gases (i.e., CO_2) through sea ice [*Delille*, 2006].

[5] Brine drainage causes the sea ice salinity to vary in time. First-year (FY) ice is initially quite saline (from 6 to 15‰), but it desalinates quickly and acquires a C-shape vertical salinity profile [*Nakawo and Sinha*, 1981]. Multi-year (MY) ice is much less saline and is characterized by a fresh surface layer [*Schwarzacher*, 1959]. Despite these striking differences in salinity over time, only prescribed, steady and simplified sea ice salinity profiles have been included into the standard sea ice models used in climate studies [e.g., *Fichefet and Morales Maqueda*, 1997; *Bitz and Lipscomb*, 1999].

[6] In the present work, we use the newly developed *Vancoppenolle et al.* [2006] (hereafter referred to as VBF06) halo-thermodynamic sea ice model, forced by climatological forcing data, to study the temporal evolution of the salinity and brine volume profiles of undeformed Arctic FY and MY ice. In addition, we discuss results from sensitivity experiments to investigate the main features of the modeled desalination. We also examine how the ice thickness is affected by the representation of the salinity profile in the model. Finally, we assess the contributions of ice growth and brine drainage to the ice-ocean salt flux.

2. Model

[7] The model is described in details in VBF06. It is a multilayer one-dimensional halo-thermodynamic sea ice model. Its prognostic variables are: ice thickness, snow thickness and both ice temperature and salinity vertical profiles. Brine volume is diagnosed from temperature and salinity. Warm temperatures and/or high salinities result in high brine volume. The temporal evolution of salinity and temperature are coupled in the following way. The evolution of the salinity profile influences the thermal properties of sea ice (i.e., specific heat, thermal conductivity and energy of melting, defined as the energy required to melt a unit volume of sea ice). These thermal properties control the heat transport and storage (thus the temperature profile) as well as the growth/melt rates at the ice interfaces (thus the ice thickness).

[8] The model ice salinity profile $S(z,t)$ varies due to 1) brine entrapment during ice growth (larger growth rates yield more salt entrapment), 2) brine expulsion (depending on the temporal derivative of ice temperature), 3) gravity drainage (assumed to depend on the vertical temperature gradient, and active if the brine network is open), and 4) flushing. Brine entrapment, expulsion and gravity drainage are modeled following *Cox and Weeks* [1988] with small differences described in VBF06. The flushing parameterization is newly developed by VBF06, so we describe it briefly here. If the brine pocket network is interconnected, corresponding to a brine volume $e \geq e_T$ = 5%, where e_T is

[1]Institut d'Astronomie et de Géophysique G. Lemaître, Université Catholique de Louvain, Louvain-la-Neuve, Belgium.

[2]Department of Atmospheric Sciences, University of Washington, Seattle, Washington, USA.

0094-8276/06/2006GL028342$05.00

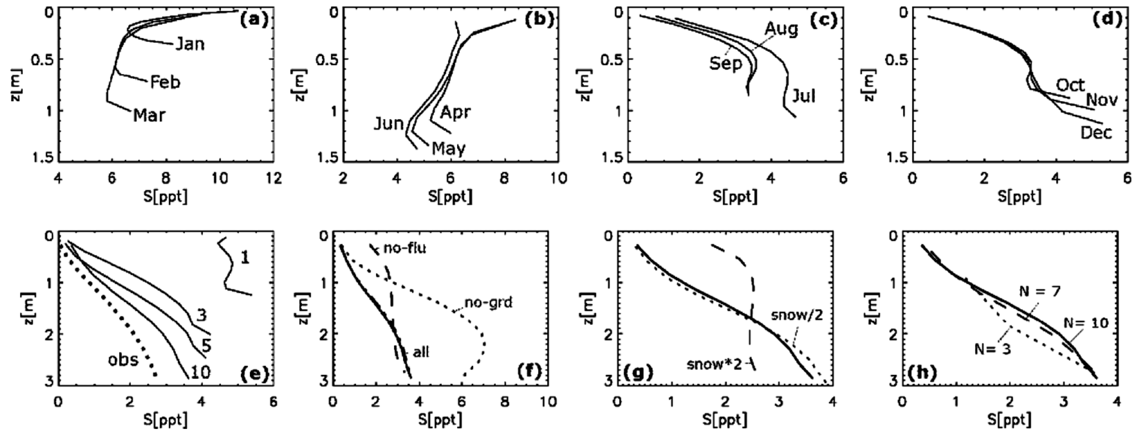

Figure 1. (a–d) Salinity profiles for the first year of the simulation, on the 15th of each month. (e) Simulated annual mean salinity profiles for years 1, 3, 5 and 10. The dotted line represents the observed MY ice salinity profile of *Schwarzacher* [1959]. Sensitivity of the annual mean salinity profile for the 10th year of the simulation to different model features: (f) Sensitivity to the different brine drainage mechanisms. Gravity drainage and flushing are turned off independently. The effect of turning off brine expulsion is too small to be visible. (g) Sensitivity to snowfall rate. Salinity profile with normal snowfall rate (solid line), half snowfall rate (dotted line) and double snowfall rate (dashed line) are shown. (h) Sensitivity to the number of vertical layers in the ice N. N = 3 (dotted line), N = 7 (dashed line) and N = 10 are plotted.

the permeability threshold mentioned by *Golden et al.* [1998], and if (2) the surface temperature $T_{su} = 0°C$, we suppose that a fraction ϕ of the available meltwater (inferred from the surface melt rate) instantaneously flows through the brine channels, replacing salty brine by surface meltwater. The meltwater salinity is given by the salinity of the snow/ice from which it formed. The snow is assumed to be of zero salinity. ϕ (= 0.30 if flushing occurs and 0 otherwise) was calibrated in VBF06. The remainder of the meltwater is assumed to contribute to lateral drainage to ocean through cracks and leads, or to collect in the lowest gravity areas and form melt ponds. The model was shown to be sensitive to ϕ and e_T values.

[9] The model is forced by idealized climatological atmospheric and oceanic conditions, which are widely used in the literature [e.g., *Maykut and Untersteiner*, 1971; *Bitz and Lipscomb*, 1999]. The monthly values of upper surface forcing data (downwelling radiative and turbulent heat fluxes) are typical of the central Arctic. The ocean-ice heat flux is set to 2 Wm^{-2} and the seasonal snow accumulation allows the snow to reach a depth of 37 cm at the end of the ice growth season. The model is initialized with 10 cm-thick sea ice and no snow. The ice is initially isosaline with S = 12‰ and isothermal with T = 270 K. The initial salinity is obtained from empirical thickness–bulk salinity relationships [*Kovacs*, 1996]. The key parameters of the thermodynamic component are as in the work by *Bitz and Lipscomb* [1999]. The only exception is i_0, the coefficient partitioning the solar radiation into surface versus internal warming equals zero if snow is present and 0.17 otherwise. 10 layers in the ice and 1 layer in the snow are used.

[10] In addition to a simulation with the prognostic halodynamic component (referred to as SZT), we also run simulations with prescribed, time-independent salinity profile. We either let the ice be isosaline with S = 4.6‰ (case BK), a value representative of typical mid-minter FY ice, or we prescribe a vertically varying salinity profile (case PR, see Figure 1e). The latter is taken from observations of MY ice in central Arctic [*Schwarzacher*, 1959]. The model simulations are summarized in Table 1.

[11] The model is run for 50 years. The annual net ice growth is less than 1 cm after 30 years for SZT, after 48 years for BK and after 27 years for PR. Annual bulk salinity variations are less than 0.01‰ after 10 years. At this time, the ice salinity reaches a quasi-equilibrium, but only stabilizes when the ice thickness is in equilibrium. Since the age of Arctic sea ice rarely exceeds 10 years [e.g., *Belchansky et al.*, 2005], we analyze the results during the first 10 years, when the model is not in equilibrium.

[12] VBF06 verified the model with a 2-year integration by forcing with daily-varying meteorological data and comparing with sea ice measurements taken from nearby landfast cores. In this study we investigate the longer-term response instead, so we force the model by repeating a climatological mean annual cycle and compare with basin-average estimates of sea ice salinity. Though neglecting ice motion and variable forcing, this idealized study offers insight into the long-term thermal and haline coupling in isolation. Future studies will investigate the influence of sea ice dynamics and synoptic variability on the coupling.

3. Results

3.1. FY Ice Salinity Variations

[13] The monthly desalination for the entire first year in the model is shown in Figures 1a–1d. Figure 2a illustrates the tendency terms of the salinity equation. The desalination of FY ice occurs in 3 phases. First, a rapid (15 days) and intense (5‰) desalination occurs during the initial rapid ice

Table 1. Description of the Simulations

Experiment	Description
SZT	prognostic halodynamic component used
PR	steady-state, vertically-varying salinity profile
BK	steady-state, isosaline salinity profile

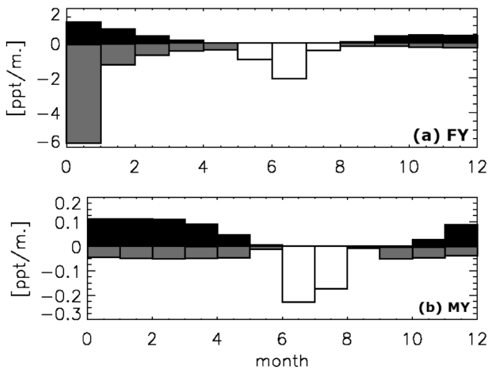

Figure 2. Monthly tendency terms of the salinity equation averaged over all vertical layers [‰/month] for (a) FY and (b) 10-year-old MY ice. Salt entrapment (black), gravity drainage (grey) and flushing (white) are plotted. Brine expulsion is too small to be visible (max. 0.03 ‰/month).

growth. This *initial desalination* (see Figure 1a, January profile) is due to gravity drainage (99% of the total desalination) throughout all the ice layers. The brine network is permeable and filled with brine denser than the seawater underneath, an inherently unstable situation. This phase lasts until an inner layer becomes cold and fresh enough so that its brine volume falls under the 5% permeability threshold. The bulk salinity decreases by 4.62‰ in this phase. This initial drainage was observed in the field by *Nakawo and Sinha* [1981] and in lab experiments by *Worster and Wettlaufer* [1997].

[14] In the second phase, the desalination pattern moves to a steady *winter regime* (see Figures 1a and 1b, February to May profiles). At this stage, the ice slab is split into two parts. The lower third is warm and saline enough so that the brine volume is above the permeability threshold and brine continues to be expelled from the ice by gravity drainage. During this phase, the bulk salinity decreases by 3.91‰. The bottom permeable region can be seen as a macroscopic representation of the brine desalination network, with smaller brine tubes joining each other in larger brine channels, as observed by *Bennington* [1967].

[15] In contrast to the lower permeable part, the upper part is impervious and therefore not connected anymore to the ocean. Only brine expulsion is active there. Though in this part brine expulsion has a high relative importance, it lowers the bulk salinity by only 0.25‰ over all winter months. However, in reality this upper part might be prone to stronger expulsion episodes associated with cold events unresolved by the monthly forcing. Such episodes could lead to the formation of frost flowers [see, e.g., *Martin et al.*, 1995]. Entrapment of salt at the ice bottom progressively slows as the ice growth rate decreases. This winter regime lasts until the end of May, resulting in a C-shaped profile as observed by *Nakawo and Sinha* [1981].

[16] The onset of surface melt and flushing marks the beginning of the third phase, or *summer regime*, in mid-June (day 162) (see Figures 1b and 1c, June to September profiles), when the whole ice layer becomes permeable. The transition between the FY C-shaped profile to the typical MY ice profile with a fresh surface layer takes around 15 days and continues to evolve slowly until mid-August (day 220), when the surface melt stops. The surface desalination pattern looks very similar to the one observed in the field by *Tucker et al.* [1987] and was observed in lab experiments by *Cottier et al.* [1999]. At freeze onset (near the end of September), the desalination process returns to the *winter regime*, but the salinity remains low at the surface (see Figure 1d).

3.2. MY Ice Salinity Profile and Its Sensitivity to Several Model Features

[17] After vigorous desalination in the first years, the salinity profile simulated by the model reaches a quasi-equilibrium by 10 years into the simulation, and the amplitude of the annual cycle is less than 0.5‰ in any layer. The simulated annual mean MY ice salinity profile is slightly more saline than the observed profile (see Figure 1e). Since errors in salinity from drainage during ice coring are about 1‰ [*Notz et al.*, 2005], there is little hope of distinguishing error in the model physics from undersampling and observational issues.

[18] Desalination slows over time as there is less salt to lose. In the second year, the total bulk salinity tendency is only 12% of its value for the first year. This amount decreases to 4% in year 5 and to 2% in year 10. Gravity drainage loses its effectiveness more quickly than flushing. In the second year, the total bulk salinity tendency due to flushing (gravity drainage) is equal to 56% (6%) of its value in year 1. Nevertheless, in the bottommost ice layers, gravity drainage remains of significant importance even for MY ice.

[19] The relative importance of brine drainage mechanisms in shaping the MY ice profile is investigated by successively eliminating each from the model (see Figure 1f). Expulsion of brine proves again to be of very minor importance, with a contribution smaller than 1%. Gravity drainage is important in winter in the lower portion of the ice, where layers are permeable. Without it, the ice is more saline in the lower two-thirds of the slab. Summertime flushing freshens the surface and transports salinity downwards.

[20] In order to assess the influence of the snow cover, we successively divide and multiply the snowfall rate by two (see Figure 1g). If snowfall is smaller, then the ice grows faster in winter and the entrapment of salt at the ice base is larger than in the control run. The desalination mechanisms are affected by a negligible amount so the bottom salinity is slightly higher in the half-snowfall simulation. Conversely, if snowfall is increased, the surface layers remain cold in summer and the permeability threshold is reached rather late in summer. The surface desalination associated with flushing operates only over a limited time (two weeks instead of two months). Thus, the MY surface salinity is greater in the double-snowfall simulation. The number of vertical ice layers can be as low as three and the model still captures the MY ice salinity profile reasonably well (see Figure 1h).

3.3. Impact of a Prognostic Salinity on Ice Thickness

[21] In this section, we study how the account for salinity variations in the model affects other model variables. Figure 3a shows the temporal evolution of ice thickness in the SZT, PR and BK simulations. The salinity-induced thickness variations are dominated by the ice thickness-growth feedback [*Vancoppenolle et al.*, 2005]. Since the

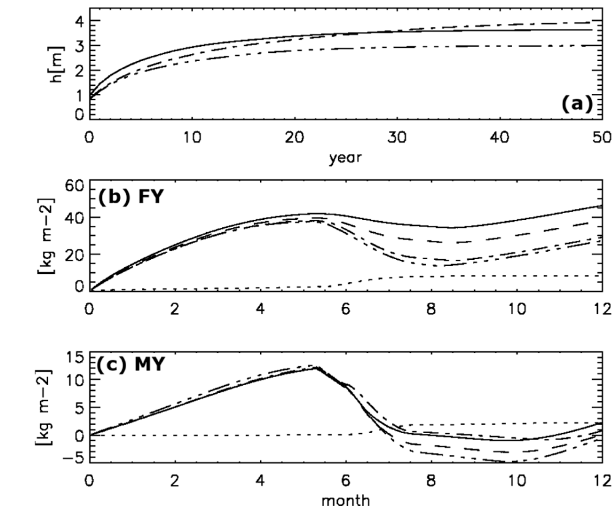

Figure 3. (a) 50-year long time series of annual mean ice thickness in the SZT (solid line), BK (dash-dotted line) and PR (dash-3x dotted line) simulations. Time-integrated massive salt flux I^s from the ice to the ocean for (b) FY and (c) 10-year-old MY ice. Total salt flux (solid line), salt flux from brine drainage (dotted line), equivalent salt flux from freshwater storage in the ice (dashed line) for SZT simulation and total salt flux for BK (dash-dotted line) and PR (dash-3x dotted line) simulations are shown.

sea ice thermal properties are salinity dependent, the differences in the ice salinity profile result in small differences in ice thickness. These differences are later amplified through a growth rate, which strongly depends on ice thickness.

[22] After 10 years into the simulation, the annual mean ice thickness in PR, BK and SZT is equal to 2.29, 2.53 and 2.85 m, respectively. PR has the thinnest ice throughout the simulation. The amplitude of the ice thickness seasonal cycle is larger in PR than in SZT and BK. The absolute difference in total melt (largely dominated by surface melt) between PR and the two other runs dominate the absolute difference in growth throughout the simulation.

[23] During the first 25 years, the ice thickness in SZT is larger than in BK. After this, the ice thickness in BK becomes larger, through the end of the simulation. The SZT integration traps more brine during growth, so it grows thicker at a faster rate than the BK case. The total (and surface) melt in SZT is less than in the BK simulation, because the fresher ice in SZT has a higher energy of melting near the surface. But after 5 years, the reduction in the ice specific heat near the surface (induced by surface freshening) in SZT dominates, and therefore, the ice melts faster.

3.4. Salt Flux to the Ocean

[24] Here we evaluate the seasonal cycle of ice-ocean brine exchange. In coupled ice-ocean models, an ice-ocean salt flux is used to ensure salt conservation in the ice-ocean system. No actual water mass is exchanged between ice and ocean when a phase change occurs. Instead fresh water or brine exchange is converted into an equivalent salt flux. In practise, dynamical effects also must be taken into account as sea ice may grow in one place and melt in another. Our 1-d model estimates only takes into account the separation of growth and melt in time not in space. However, the following equations apply more generally.

[25] The ice-ocean salt flux F^s_{tot} (>0 from the ice to the ocean, in kg m^2 s^{-1}) can be divided into two parts: $F^s_{tot} = F^s_{bd} + F^s_{up}$. The first component is a direct salt flux from all processes which we can refer to as *brine drainage*:

$$F^s_{bd} = -\rho[h\frac{dS}{dt}|_{bd} + (S_w - S_b)\frac{dh}{dt}|^{>0} - S\frac{dh}{dt}|^{<0}]. \qquad (1)$$

ρ is the sea ice density, h is the ice thickness, S_w is the seawater salinity and S_b is the salinity of new ice. The first term in (1) corresponds to all brine drainage mechanisms. The next two account for salt lost by the ocean via brine entrapment during ice growth and for salinity returned to the ocean during ice melt. The second component of the ice-ocean salt flux is from freshwater exchange between the sea ice slab (including snow) and ocean due to melting or growing, which we refer to as *net freshwater uptake*:

$$F^s_{up} = \rho_s S_w(1-\phi)\frac{\partial h_s}{\partial t}|^{<0} + \rho_i S_w(1-\phi)\frac{\partial h_i}{\partial t}, \qquad (2)$$

where ρ_s is the snow density, h_s is the snow depth, and ϕ is the partitioning coefficient for flushing. The first term in (2) represents the direct freshwater input from snow melt. The second term corresponds to the ice growth-induced freshwater removal from the ocean (or ice melt-induced freshwater return to the ocean).

[26] We associate these salt fluxes with the *integrated massive salt* flux at day d, $I^s_{tot}(d) = \int_{1Jan}^{d} F^s_{tot}(t)dt$. Similarly, the two components $I^s_{bd}(d)$ and $I^s_{up}(d)$ are defined as the temporal integrals of $F^s{}_{bd}$ and $F^s{}_{up}$. Their contribution to the net ice-ocean I^s_{tot} are very different for FY ice and MY ice (see Figure 3). For FY ice surviving one summer, the total amount of salt rejected from the ice is around 45 kg m^{-2} over a year, and almost four fifths of this amount is supplied by the net freshwater uptake in the ice. For MY ice, over a year, there is almost no net salt rejection from the ice to the ocean. But integrated over winter only, the freshwater uptake in MY ice rejects almost 10 kg m^{-2} of salt. In contrast, the brine drainage in MY ice has an annual contribution of 2 kg m^{-2}.

[27] In Figures 3b and 3c, the total salt flux to the ocean is shown for the PR and BK simulations. For FY ice surviving one summer, the total salt rejection over a year in SZT is 15 kg m^{-2} higher than in PR and BK. The contribution of $I^s{}_{up}$ accounts for 68% of the average difference in $I^s{}_{tot}$, while the remainder is from brine drainage. The differences essentially build over summer. For MY ice, the differences between the three simulations are only significant in summer, and their magnitude is always smaller than 5 kg m^{-2}.

4. Discussion and Conclusions

[28] We presented here a simulation of the salinity profile of undeformed Arctic sea ice with a multi-layer halo-thermodynamic sea ice model. The model successfully reproduces the FY ice desalination, which we divided in three steps, referred to as initial, winter and summer stages of desalination. The intensity of brine drainage decreases

from year to year and the desalination continues until a quasi equilibrium is reached on year 10. The modeled MY ice salinity profile compares well with observations.

[29] The modeled desalination is sensitive to gravity drainage in the bottom layers and to flushing in the uppermost layers. If snowfall increases by a sufficient amount, the upper ice layers are thermally insulated and cannot reach the permeability threshold of 5%, preventing flushing to occur, and keeping the upper part of the ice slab saline. Using 5 vertical ice layers is largely sufficient to simulate the key features, which is the maximum current number used in large-scale sea ice models [e.g., *Hunke and Lipscomb*, 2004]. To incorporate our halo-thermodynamic model in a large-scale sea ice model would require to include the mass of salt for each vertical ice layer in the advection scheme and to add the brine drainage contribution to the ice-ocean salt flux.

[30] Substantial differences in ice thickness occur when different parameterizations of salinity are used. They are driven by differences in salinity at both interfaces, which affect the growth and melt rates. The transient and equilibrium sensitivities of the modeled ice thickness are different. The effect of modeling sea ice desalination on ice-ocean salt/freshwater accounts for 15 kg m^{-2} (a third) of the total annual salt rejected by FY ice. This effect is an order of magnitude smaller for MY ice.

[31] Our results also indicate a limited picture of how the ice-ocean salt exchanges could be affected by a transition to a seasonal ice cover, often cited as a possible scenario for the next century [e.g., *Stroeve et al.*, 2005]. The increased winter ice growth would enhance the total ice-ocean salt flux compared to now, and the summer meltwater inflow would also be larger during summer melt, amplifying the sea ice-induced seasonal cycle of mixed-layer salinity. In conclusion, our study demonstrated that including a halodynamic component would significantly improve the next generation of large-scale sea ice models.

[32] **Acknowledgments.** Martin Vancoppenolle is Research Assistant at the Belgian National Fund for Industrial and Agricultural Research and is supported by the Belgian Federal Science Policy Office. This study was carried out within the scope of the project A Second-Generation Model of the Ocean System, funded by the Communauté Française de Belgique (ARC 04/09-316). We thank Valérie Dulière, Hugues Goosse and Bruno Tremblay for helpful discussions on various aspects of this work and two anonymous reviewers for careful review of the manuscript.

References

Ackley, S. F., and C. W. Sullivan (1994), Physical controls on the development and characteristics of Antarctic sea ice biological communities—A review and synthesis, *Deep Sea Res.*, *41*, 269–281.

Arzel, O., T. Fichefet, and H. Goosse (2006), Sea ice evolution over the 20th and 21st centuries as simulated by current AOGCMs, *Ocean Modell.*, *12*, 401–415.

Belchansky, G. I., D. C. Douglas, and N. G. Platonov (2005), Spatial and temporal variations in the age structure of Arctic sea ice, *Geophys. Res. Lett.*, *32*, L18504, doi:10.1029/2005GL023976.

Bennington, K. O. (1967), Desalination features in natural sea ice, *J. Glaciol.*, *6*, 845–857.

Bitz, C. M., and W. H. Lipscomb (1999), An energy-conserving thermodynamic model of sea ice, *J. Geophys. Res.*, *104*, 15,669–15,677.

Cottier, F., H. Eicken, and P. Wadhams (1999), Linkages between salinity and brine channel distribution in young sea ice, *J. Geophys. Res.*, *104*, 15,859–15,871.

Cox, G. F. N., and W. F. Weeks (1988), Numerical simulations of the profile properties of undeformed first-year sea ice during growth season, *J. Geophys. Res.*, *93*, 12,449–12,460.

Delille, B. (2006), Inorganic carbon dynamics and air-ice-sea CO_2 fluxes in the open and coastal waters of the Southern Ocean, Ph.D. thesis, 297 pp., Univ. of Liège, Liège, Belgium.

Fichefet, T., and M. A. Morales Maqueda (1997), Sensitivity of a global sea ice model to the treatment of ice thermodynamics and dynamics, *J. Geophys. Res.*, *102*, 12,606–12,646.

Golden, K. M., S. F. Ackley, and V. I. Lytle (1998), The percolation phase transition in sea ice, *Science*, *282*, 2238–2241.

Hunke, E. C., and W. H. Lipscomb (2004), CICE: The Los Alamos Sea Ice Model Documentation and Software User's Manual, Los Alamos Natl. Lab., Los Alamos, N. M.

Kovacs, A. (1996), Sea ice, part I. Bulk salinity versus ice floe thickness, *CRREL Rep.*, *96-7*, 16 pp., Cold Reg. Res. and Eng. Lab., Hannover, N. H.

Martin, S., R. Drucker, and M. Fort (1995), A laboratory study of frost flower growth on the surface of young sea ice, *J. Geophys. Res.*, *100*, 7027–7036.

Maykut, G. A., and N. Untersteiner (1971), Some results from a time-dependent model of sea ice, *J. Geophys. Res.*, *76*, 1550–1575.

Nakawo, M., and N. K. Sinha (1981), Growth rate and salinity profile of first-year sea ice in the high Arctic, *J. Glaciol.*, *27*, 315–331.

Notz, D., J. S. Wettlaufer, and M. G. Worster (2005), A non-destructive method for measuring the salinity and solid fraction of growing sea ice in situ, *J. Glaciol.*, *51*, 159–166.

Schwarzacher, W. (1959), Pack-ice studies in the Arctic Ocean, *J. Geophys. Res.*, *64*, 2357–2367.

Stroeve, J. C., M. C. Serreze, F. Fetterer, T. Arbetter, W. Meier, J. Maslanik, and K. Knowles (2005), Tracking the Arctic's shrinking ice cover: Another extreme September minimum in 2004, *Geophys. Res. Lett.*, *32*, L04501, doi:10.1029/2004GL021810.

Tucker, W. B., A. J. Gow, and W. F. Weeks (1987), Physical properties of summer sea ice in the Fram Strait, *J. Geophys. Res.*, *92*, 6787–6803.

Vancoppenolle, M., T. Fichefet, and C. M. Bitz (2005), On the sensitivity of undeformed Arctic sea ice to its vertical salinity profile, *Geophys. Res. Lett.*, *32*, L16502, doi:10.1029/2005GL023427.

Vancoppenolle, M., C. M. Bitz, and T. Fichefet (2006), Summer landfast sea ice desalination at Point Barrow, Alaska: Model and observations, *J. Geophys. Res.*, doi:10.1029/2006JC003493, in press.

Worster, M. G., and J. S. Wettlaufer (1997), Natural convection, solute trapping, and channel formation during solidification of saltwater, *J. Phys. Chem. B*, *101*, 6132–6136.

C. M. Bitz, Department of Atmospheric Sciences, University of Washington, Seattle, WA 98195, USA.

T. Fichefet and M. Vancoppenolle, Institut d'Astronomie et de Géophysique G. Lemaître, Université Catholique de Louvain, B-1348 Louvain-la-Neuve, Belgium. (vancop@astr.ucl.ac.be)